NUCL SCI TECH (2022) 33:159
https://doi.org/10.1007/s41365-022-01136-5

Discrimination of neutron and gamma ray using the ladder gradient method and analysis of filter adaptability

Hao-Ran Liu[1,2] · Ming-Zhe Liu[1] · Yu-Long Xiao[2] · Peng Li[2] · Zhuo Zuo[1,2,3] · Yi-Han Zhan[2]

Received: 25 June 2022 / Revised: 31 August 2022 / Accepted: 16 September 2022 / Published online: 9 December 2022

Abstract This study proposes a ladder gradient method for neutron and gamma-ray discrimination. The proposed method exhibited state-of-the-art performance with low time consumption, which incorporates two parts: information extraction and discrimination factor calculation. A quasi-continuous spiking cortical model was proposed to extract information from the radiation pulse signals, thus generating an ignition map corresponding to each pulse signal. The ignition map can be used to calculate the discrimination factor. A ladder gradient calculation was introduced to obtain a discrimination factor with low computational complexity. The proposed method was compared with five other discrimination methods to evaluate its robustness and efficacy. Furthermore, the filter adaptability of the pulse-coupled neural network and ladder gradient methods was investigated. Possible reasons for adapting the conditions with different discrimination methods and filters were analyzed. Experiments were conducted in 20 filtering situations with 11 types of filters to determine the most suitable filters for discrimination methods. The experimental results revealed that the three most adaptive filters of the pulse-coupled neural networks and ladder gradient methods are the wavelet, elliptic, and median filters and the elliptic, moving average, and wavelet filters, respectively.

Keywords n-γ Discrimination · Pulse-shape discrimination · Ladder gradient · Pulse-coupled neural network · Filtering · Filter adaptability

1 Introduction

Neutrons have been used in many scientific fields since they were discovered by Chadwick in 1932, making neutron detection technology vital for a variety of applications. Examples include nuclear reactors [1, 2], meteorology [3], national security [4, 5], astronautics [6], biology [7], and radiopharmaceuticals [8]. Detecting neutrons and monitoring neutron flux are vital tasks in the aforementioned fields. However, several radiation detectors that are sensitive to neutrons are additionally sensitive to high-energy photons (gamma rays). These photons inevitably accompany neutrons because of their interaction with the surrounding environment. This concomitant phenomenon causes difficulty in detecting neutrons because detectors retrieve the radiation pulse signals of neutrons and gamma rays simultaneously, making it particularly difficult to count only neutrons per unit of time. To overcome this obstacle, researchers have attempted to discriminate neutrons and gamma rays through their different interaction characteristics with the sensitive volume of a radiation detector, which can be presented by the differences in the pulse shapes of these two particles [9]. Based on this

This work was supported by the National Natural Science Foundation of China (Nos. U19A2086, 41874121, 12205078).

✉ Ming-Zhe Liu
liumz@cdut.edu.cn

[1] State Key Laboratory of Geohazard Prevention and Geoenvironment Protection, Chengdu University of Technology, Chengdu 610059, China

[2] The Engineering & Technical College of Chengdu University of Technology, Leshan 614000, China

[3] Southwestern Institute of Physics, Chengdu 610225, China

discrimination principle, the pulse-shape discrimination (PSD) technique has been developed [10, 11], which has been commonly used in numerous scientific fields to satisfy the neutron detection requirements [12, 13]. One of the most important components of the PSD technique is its discrimination algorithm. This algorithm is responsible for the information extraction process of each radiation pulse signal, generating a discrimination factor for each signal, which is used to separate the neutron and gamma-ray pulse signals (n-γPSs).

Many discrimination methods have emerged during the past decades, such as the most commonly used charge comparison (CC) method [14], fast discrimination-capable zero-crossing (ZC) method [15, 16], frequency-domain-based frequency gradient (FGA) method [17] and fractal spectrum method [18]. The CC method is among the most frequently used PSD methods. It exhibited good discrimination performance under various conditions with low time consumption. The most significant advantage of the ZC method is its low computational complexity, making it a better option for real-time discrimination tasks. However, the discrimination performance of the ZC method is usually unsatisfactory because its information extraction process is too simple to fully determine the differences between pulse signals. Frequency-domain-based methods play an essential role in high-noise scenarios. Nevertheless, their computational burden is usually high and they require a long signal-processing time. In 2021, Liu et al. proposed a novel discrimination method with outstanding discrimination performance [19], introducing a pulse-coupled neural network (PCNN) into the neutron and gamma-ray pulse-shape discrimination field for the first time. The PCNN displayed breakthrough discrimination performance and significantly outperformed conventional discrimination algorithms, such as the CC and ZC methods. The outstanding discrimination effect of the PCNN was attributed to its dynamic information extraction ability. As a biological neurology research-based neural network, the PCNN was initially conceived to imitate the working style of the biological neuron cortex to obtain the capability of processing dynamic information from pictures or videos [20]. In the biological visual system, when external light sources stimulate photoreceptor cells in the retina, these cells generate electrical signals (spikes) and relay these spikes to the adjacent optic nerves. These electrical signals stimulate neurons in the cortex, causing further spike generation and transmission between cell assemblies [21, 22]. Biological neurology research has corroborated that this spike behavior between cell assemblies can recognize the information contained by the original stimuli received by the photoreceptor cells and makes the brain understand features, details, and other information in images or videos [23]. Inherited from this working style, the PCNN can similarly extract the dynamic information of images. As the PCNN was proposed by Johnson et al. in 1994, it has been used in numerous image-processing fields [24]. Examples include object recognition [25, 26], image shadow removal [27], and image feature extraction [28].

Although Liu et al. demonstrated the discrimination effect of this PCNN-based method [29], its high computational complexity limited its rapid discrimination applications. This computational burden is a result of two factors: the high number of iterations of the PCNN and the integration process of the ignition map. Consequently, the computational burden of the PCNN-based discrimination method should be reduced, which requires a novel discrimination technique with a high information extraction ability and low computational complexity. In this study, a ladder gradient (LG) method was proposed. It replaces the integration process of the PCNN-based method with ladder gradient calculations. Moreover, a quasi-continuous spiking cortical model (QC-SCM) was proposed to generate ignition maps required for the ladder gradient calculation process. The QC-SCM can achieve a better-detailed information extraction performance and noise-processing ability than the PCNN, with fewer number of iterations and manual parameters. Experiments were conducted to compare the discrimination results of the LG method with those of the other five conventional discrimination methods to evaluate the proposed method's efficiency and robustness.

Furthermore, the filtering process is a vital step in most PSD algorithms, that is, reducing the noise level of n-γPSs and improving the discrimination performance. However, there are many optional filtering methods in the signal-processing field. Zuo et al. revealed that various discrimination performances were presented for different discrimination methods when coupled with various filtering methods [30]. Consequently, several filtering methods with the best discrimination performance were identified for each discrimination algorithm. However, the filter adaptability of PCNN has not yet been investigated. The most suitable filtering method for PCNN is unknown. To determine the most appropriate filtering method for the PCNN and the newly proposed LG methods, we conducted experiments to validate the performances of nearly every standard filtering method in the PSD field when coupled with these two methods. The performance of each filter is evaluated using several objective criteria.

The layout of this study is arranged as follows. The LG discrimination method principle is elaborated in Sect. 2. The filtering methods used are described in Sect. 3. Section 4 presents the evaluation criteria used to quantify the performance of the different filtering methods. The detailed structure of the experiments and experimental results are presented in Sect. 5. Finally, in Sect. 6, the conclusions of this study are presented.

2 Fundamentals of the ladder gradient method

Figure 1 shows a flow chart of the ladder gradient (LG)-based neutron and gamma-ray discrimination process. The radiation pulse signals (n-γPSs) were first filtered to reduce the negative impact of the noise. Then, the filtered n-γPSs were fed to the quasi-continuous spiking cortical model (QC-SCM), generating ignition maps with the extracted dynamic information. Each ignition map corresponds to an n-γPS and is a vector with the same length as n-γPS. Finally, the ladder gradient value R is calculated based on the n-γPS ignition map. The ladder gradient is defined as the slope between the maximum point and the $\hat{m}$th mode after the maximum point in the ignition map, where $\hat{m}$ is an empirical parameter related to the characteristics of the radiation pulse shapes. The formula for ladder gradient R is as follows:

$$R = \frac{\mathcal{Y}_B - \mathcal{Y}_A}{\mathcal{X}_B - \mathcal{X}_A}, \tag{1}$$

where $(\mathcal{X}_A, \mathcal{Y}_A)$ and $(\mathcal{X}_B, \mathcal{Y}_B)$ are the coordinates of the maximum point and the $\hat{m}$th mode after the maximum point in the ignition map, respectively. Compared with the original PCNN, an integration process of the ignition counts corresponding to the radiation signal's falling edge and delayed fluorescence parts is used to calculate the discrimination factor. The calculation of LG's discrimination factor, that is, the ladder gradient, is much less cumbersome. However, this computational complexity release comes at the cost of higher noise sensitivity and poorer information extraction performance. This is because the influence of noise on the coordinates of the two points is significantly heavier than that on the integration of ignition maps, and the integration results contain more information

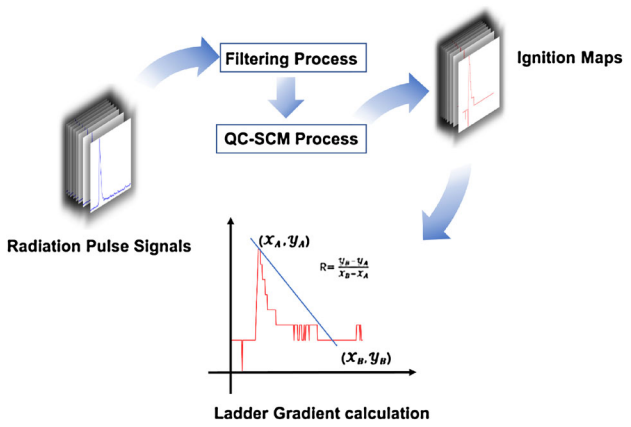

Fig. 1 (Color online) Flowchart of the ladder gradient method. The radiation pulse signals are first denoised by a filtering method. Next, the QC-SCM is used to generate the ignition maps. Finally, the discrimination factor, the ladder gradient, is calculated for each ignition map

than the slope of the two locations. Consequently, an optimized model with better anti-noise and information extraction abilities is required for the ignition process of the LG method that presents less noise and more information in the ignition maps.

LG uses QC-SCM to generate the ignition maps of n-γPSs. The QC-SCM is proposed based on recent advances in PCNN image-processing fields. Yang et al. demonstrated that the discrete PCNN model is different from the continuous characteristics of the mammalian visual cortex; therefore, it is challenging to achieve high resolution in the firing process. A non-integer step PCNN model to simulate the continuous structure of biological neurons was also proposed by them [31]. This model can better recognize detailed information and process noise from images at the cost of a relatively high computational burden compared with the original PCNN. In this study, we propose a QC-SCM that introduces a continuous structure into the spiking cortical model, a simplified version of the PCNN, to achieve a detailed processing ability and firing resolution while maintaining a low computational burden. The mathematical expression for the QC-SCM is as follows:

$$\boldsymbol{U}_{ij}(t+\Delta t) = f^{\Delta t}\boldsymbol{U}_{ij}(t) + \boldsymbol{S}_{ij}\left(1 + \sum_{kl} \boldsymbol{W}_{ijkl}\boldsymbol{Y}_{kl}(\mathrm{t})\right), \tag{2}$$

$$\boldsymbol{\theta}_{ij}(t+\Delta t) = g^{\Delta t}\boldsymbol{\theta}_{ij}(t) + h\boldsymbol{Y}_{ij}(t), \tag{3}$$

$$\boldsymbol{Y}_{ij}(t+\Delta t) = \begin{cases} 1, & \text{if } \dfrac{1}{1+\exp\left(-\left(\boldsymbol{U}_{ij}(t+\Delta t) - \boldsymbol{\theta}_{ij}(t+\Delta t)\right)\right)} > 0.5 \\ 0, & \text{otherwise} \end{cases} \tag{4}$$

where $\boldsymbol{U}_{ij}$ is the membrane potential of a neuron located at (i,j); t is the number of iterations; Δt is a parameter that determines the time continuous characteristic of QC-SCM, whose value ranges between 0 and 1; the closer it is to 0, the closer the QC-SCM is to a continuous time system; f is the attenuation coefficient of $\boldsymbol{U}_{ij}$; $\boldsymbol{S}_{ij}$ is the external stimulus, that is, the radiation pulse signal; $\boldsymbol{W}_{ijkl}$ is the synaptic weight matrix that controls the connection between the central neuron at (i,j) and its surrounding neurons at (k,l); $\boldsymbol{Y}_{ij}$ and $\boldsymbol{Y}_{kl}$ are the outputs of the spikes of neurons located at (i,j) and (k,l), respectively.$\boldsymbol{\theta}_{ij}$ is the dynamic threshold; g is the attenuation coefficient of $\boldsymbol{\theta}_{ij}$; and h is the attenuation coefficient of $\boldsymbol{Y}_{ij}$.

Figure 2 shows a comparison of the pulse signals and ignition maps. The difference between the neutron and gamma-ray signals appeared in the falling edge (approximately 90 ns) and delayed fluorescence parts (approximately 180 ns), as shown in Fig. 2a. This difference was successfully captured and amplified by the PCNN, as shown in Fig. 2b, with generally higher ignition times in these two parts. However, the ladder shape ignition maps

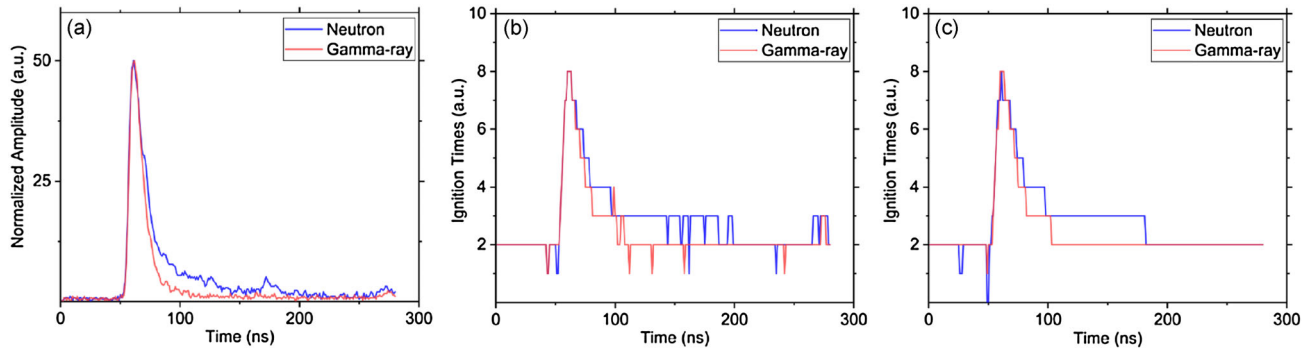

Fig. 2 (Color online) Comparison between pulse signals and ignition maps. **a** Neutron and gamma-ray pulse signals; **b** Ignition maps generated by the PCNN; and **c** ignition maps generated by the QC-SCM

were unstable, with many fluctuations ranging from 100 to 200 ns. This fluctuation is caused by noise introduced by the radiation detection system. Although an integration process for the falling edge and delayed fluorescence parts can compensate for the noise-induced fluctuation, the computational complexity increment is an inevitable cost.

In contrast, the QC-SCM ignition maps, as shown in Fig. 2c, did not show fluctuations in the ladder shapes. This stabilized ladder shape is formed because of the better noise-processing ability of the QC-SCM than that of the PCNN. A more computationally convenient discrimination factor than the integration, the ladder gradient, can be used because of the smooth ladder shape. Moreover, the QC-SCM can achieve a similar difference amplification performance as that of the PCNN with fewer iterations because of its better-detailed information extraction ability. The number of QC-SCM manual parameters is much lower than that of the PCNN. Similar to the PCNN, the QC-SCM requires no training process before discrimination.

3 Filtering methods

A one-dimensional signal can be considered a useful signal superposed by white Gaussian noise:

$$s(n) = j(n) + ke(n), \tag{5}$$

where n is the time, s is the one-dimensional signal, j is the useful signal, and ke is the Gaussian noise.

In practical applications, sampled signals are discrete-time signals with equal time steps. Consequently, $s(n)$ can be denoted by an N-dimensional random vector:

$$s(n) = \begin{pmatrix} j(0) + \sigma e(0) \\ j(1) + \sigma e(1) \\ j(2) + \sigma e(2) \\ \vdots \\ j(N-1) + \sigma e(N-1) \end{pmatrix} = \begin{pmatrix} j(0) \\ j(1) \\ j(2) \\ \vdots \\ j(N-1) \end{pmatrix} + \begin{pmatrix} ke(0) \\ ke(1) \\ ke(2) \\ \vdots \\ ke(N-1) \end{pmatrix}. \tag{6}$$

The noise removal process extracts the useful signal $j(n)$ from the original signal $s(n)$. There is a significant difference between the conventional de-noising process and n-γ PS noise process. For the discrimination application of neutrons and gamma rays, slight, sometimes even conspicuous, distortion of the denoised signal is acceptable if the pulse shape difference between neutrons and gamma rays is amplified. Filters with fewer signal distortions are preferred under the same discrimination performance.

In this study, a total of 11 filtering methods and 20 filtering conditions were investigated to determine the optimal filters for the PCNN and LG methods. The details of these filtering methods are presented in Section S1 of Supplemental Information. These methods incorporate the Butterworth filter [32, 33], Chebyshev filter [34, 35], elliptic filter [36], median filter [37], moving average filter [38, 39], Fourier filter [40], wavelet filter [41–44], Wiener filter [45, 46], least mean square adaptive filter [47], morphological filter [48, 49], and windowed-sinc filter [50, 51].

4 Evaluation criteria

4.1 Figure of merit

The figure of merit (FoM) is a standard measurement used to evaluate the discrimination effect of neutrons and gamma rays [52]. The calculation of FoM first draws a histogram of discrimination results, which contains two groups corresponding to the gamma ray and neuron counts. Then, a Gaussian fitting function is used to fit these two groups, forming a fitting curve that can be further used to calculate the distance between these two peaks, s and the full width at half maximum of each group. Finally, the FoM is defined by the following equation:

$$\mathrm{FoM} = \frac{S}{\mathrm{FWHM}_n + \mathrm{FWHM}_\gamma}, \tag{7}$$

where FWHM_n and FWHM_γ denote the full width at half maximum of the neutron and gamma-ray groups, respectively. If the discrimination performance is good, the distance s should be significant, and both FWHM_n and FWHM_γ should be small. The larger the FoM, the better the discrimination performance.

4.2 Denoised signal similarity measurements

There are several objective measurements of the denoising performance in image noise removal applications [53]. They can also be calculated in the one-dimensional condition to evaluate the de-noising performance of the radiation signals.

The peak signal-to-noise ratio (PSNR) measures the similarity between the denoised signal $y(n)$ and the original signal $s(n)$ and is defined as

$$\mathrm{PSNR} = 10\log_{10}\left(\frac{N^2}{\mathrm{MSE}}\right), \tag{8}$$

where N is the length of the original signal, and the mean square error (MSE) is defined as

$$\mathrm{MSE} = \frac{1}{N}\sum_{n=1}^{N}[s(n) - y(n)]^2. \tag{9}$$

The root mean square error (RMSE) can be calculated as

$$\mathrm{RMSE} = \sqrt{\mathrm{MSE}}. \tag{10}$$

The DIV can be used to measure the de-noising performance, which is defined as

$$\mathrm{DIV} = \left|1 - \frac{\sigma_y^2}{\sigma_s^2}\right|, \tag{11}$$

where σ_y and σ_s represent the variance of the denoised and original signals, respectively.

Shannon entropy (SE) is a concept in information theory that can represent the average information contained in a signal [54, 55]. It can be estimated as

$$\mathrm{SE} = -\sum_n s^2(n)\log\left(s^2(n)\right). \tag{12}$$

By calculating the SE of $s(n)$ and $y(n)$, the entropy difference (ED) was obtained as follows:

$$\mathrm{ED} = |\mathrm{SE}(s) - \mathrm{SE}(y)|, \tag{13}$$

when the values of MSE, RMSE, and DIV are closer to 0, and the PSNR value is considerable, and the denoised signal is similar to the original signal, indicating a better filtering result with less signal distortion. When the value of ED is smaller, the amount of information corrupted in the filtering process is less; hence, the filtering results are better.

4.3 Time consumption

The time consumption of the LG method and several other discrimination methods to process 9414 radiation pulse signals was measured. Furthermore, the time consumed by each filter to process all the signals was measured. Time consumption represents the computational complexity of the discrimination and filtering methods, indicating their implementation viability.

4.4 Discrimination accuracy

Determine whether the discrimination accuracy is influenced when n-γPSs have been smoothed by a filter is crucial. We recorded the total neutron pulse signal counts (N-count) and gamma-ray pulse signal counts (G-count) from each filter discrimination result. Furthermore, the discrimination results of the Fourier filter-processed signals were used as the standard reference. Fourier filters are widely applied in the pulse-shape discrimination field. The number of incorrectly discriminated pulse signals after processing the other filters was recorded as an error. The error ratio is defined as follows:

$$\text{Error ratio} = \frac{\text{Error}}{\text{Total number of signals}}. \tag{14}$$

Smaller values of error and error ratio indicate better results.

5 Experimental procedures

5.1 Experiment equipment and parameter settings

This study used a ^{241}Am-Be isotope neutron source with 4.5 MeV average energy to produce the radiation-superposed field. The n-γPSs of this superposed field were collected using an EJ299-33 plastic scintillator and a digital oscilloscope (TPS2000B) with a sampling rate of 1 GS/s, a vertical resolution of 8 bits, and a bandwidth of 200 MHz. The trigger threshold was set at 500 mV, approximately corresponding to a 1.6 MeVee energy (the definition of MeVee can be found in [19]). The pulse duration was 160 ns, which does not corrupt the information inside the signals with respect to the Shannon criteria [56]. All the discrimination and filtering processes were conducted on Windows 11 using an AMD 5900X CPU. The parameters of the LG are: $\hat{m} = 20$, $t = 50$, $\Delta t = 0.5$, $\boldsymbol{W}_{ijkl} = [0.44, 0, 0.44]$, $f = 0.38$, $g = 0.8$, and $h = 8.45$.

Five methods were compared with the LG method: falling edge percentage slope (FEPS) [57, 58], zero crossing (ZC) [15, 16], charge comparison (CC) [59], frequency gradient analysis (FGA) [17], and pulse-coupled neural network (PCNN) [19]. The parameters of these discrimination methods are presented in Sect. S2.1 of Supplemental Information.

The parameters of the filtering methods used in this study were optimized to achieve the near-best performance of each filter and are presented in Sects. 2.2 and 2.3 of Supplemental Information.

5.2 Discrimination results and comparison

Figure 3 shows the discrimination performance. Discrimination is poorly performed by FEPS, as shown in Fig. 3a. Numerous pulse signals are located between the neutron and gamma-ray groups. The gradient of the two points at the peak of the signal and the end of the falling edge is used by the FEPS as the discrimination factor, similar to process of the LG method. However, without an information extraction process, noise significantly influences the discrimination performance of the FEPS. Additionally, the information inside the delayed fluorescence parts was not considered by FEPS. Consequently, it exhibits an unsatisfactory discrimination effect. Ignoring the delayed fluorescence parts influences the performance of the ZC method, as shown in Fig. 3b. Although the differentiation and integration processes help the ZC reduce noise interference, the incomplete pulse shape difference still causes a considerable negative impact, with a better Gaussian distribution of n-γ groups than that of the FEPS; however, many pulse signals are located between the two groups.

The discrimination performances of CC, FGA, and PCNN are better than those of the two aforementioned methods, as shown in Fig. 3c–e. In the results of these three methods, the n-γ groups conform to a Gaussian distribution while separating from each other. The reason for this good performance is that they consider the information contained in the delayed fluorescence parts and use the integration process to achieve anti-noise ability; the CC integrates the amplitudes of pulse signals; the FGA uses the first component of a pulse signal's Fourier transformed form, which corresponds to the average amplitude of the whole pulse signal; and the PCNN integrates the ignition times of ignition maps. However, the LG method's performance was similar to that of the three methods without the integration process, as shown in Fig. 3f. The negative impact of noise is preprocessed by the QC-SCM; therefore, no integration process is required to obtain a discrimination factor. Instead, a ladder gradient was used to significantly reduce the computational burden. It is worth noting that all discrimination methods use a Fourier filter to preprocess the pulse signals, except for the LG method. The raw pulse signals are used for the LG because the pre-denoising with the Fourier filter reduces its discrimination performance. Section 5.3 presents a detailed analysis of this phenomenon.

The results of the objective evaluation are presented in Table 1. The results of the FoM values are consistent with the intuitive presentation of three-dimensional histograms. FEPS and ZC have the worst performance, with FoM values of approximately 1. The CC and FGA performances were at the same level. LG exhibits the second-best performance with a 1.54 FoM, which is slightly lower than the 1.75 FoM of the PCNN. The time consumption of each method was defined as the total CPU processing time for the 9414 pulse signals (the time consumption of the filtering process was excluded). The LG reduced the time consumption by approximately 37% compared with that of the PCNN, approaching the level of other conventional discrimination methods. These experimental results demonstrate the efficiency and robustness of the proposed LG method, which can achieve a better performance than conventional methods without preprocessing by filters and consumes less time than PCNN. The low computational complexity of LG makes it possible to implement integrated radiation detection systems, thereby realizing real-time discrimination.

5.3 Filtering results and analysis

We conducted experiments to validate the performance of the PCNN and LG coupled with each filter mentioned in

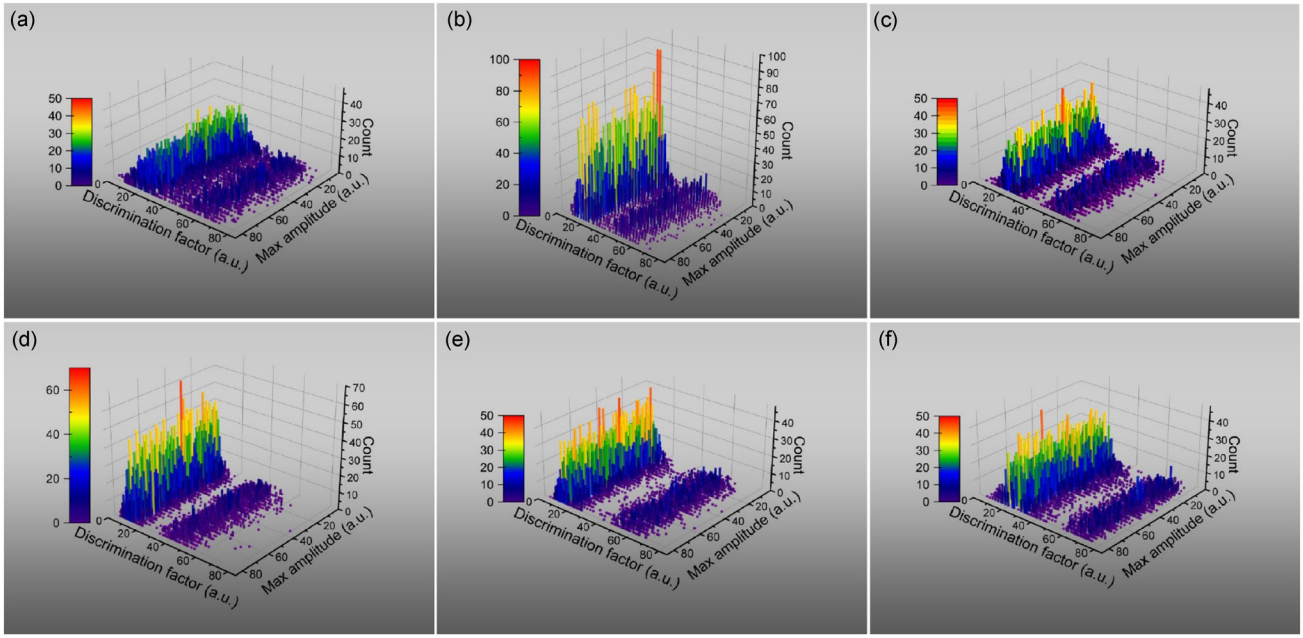

Fig. 3 (Color online) Three-dimensional histograms of discrimination results for the following methods: **a** FEPS, **b** ZC, **c** CC, **d** FGA, **e** PCNN, and **f** LG. In each histogram, the shapes of two groups conform to the Gaussian distribution and a wide and clean gap between these groups indicates good discrimination performance

Table 1 Discrimination results and time consumption (the CPU processing time for 9414 pulses)

Criteria/method	FEPS	ZC	CC	FGA	PCNN	LG
FoM (a.u.)	0.97	1.09	1.38	1.47	1.75	1.54
Time consumption (s)	1.28	1.36	1.30	1.31	2.78	1.76

Sect. 3. We evaluated their performance from four aspects: (A) discrimination performance (which is crucial in neutron and gamma-ray discrimination applications), (B) denoised signal similarity (which measures the distortion), (C) time (referring to the total CPU processing time of each filter for all 9414 pulse signals), and (D) discrimination accuracy (which uses the most widely used discrimination and filtering method, that is, the CC method with a Fourier filter, as the reference, comparing its discrimination results with the results of other filters). There is no ground truth for the discrimination results because the n-γPSs used in this study are the actual measured signals. Although the CC method with a Fourier filter has been demonstrated to be robust, its discrimination results cannot be equated to the ground truth. Consequently, discrimination was considered successful when the discrimination error ratio was under 2%.

The distortion of a signal's peak and falling edge caused by different filters is shown in Fig. 4. As shown in Fig. 4a, b, the elliptic filter displayed a maximum change in the amplitude of the peaks, and the Butterworth filter smoothed the falling edge the best. As shown in Fig. 4c, d, the median filter significantly changed the shape of the signal's peak, and the moving average filter had the best performance in smoothing the falling edge. As shown in Fig. 4e, f, the distortion of the peak in all three methods remains at the same level, whereas the wavelet filter outperforms the others in smoothing the falling edge. As shown in Fig. 4g, h, although the falling edges show the same characteristics after processing three different LMS filter conditions, the peak distortion of the model-reference condition is more extensive than that of the others. As shown in Fig. 4i, j, the morphological filters completely changed the characteristics of the pulse shapes with different peak shapes and locations. Finally, as shown in Fig. 4k, l, the model-reference Wiener filter significantly distorted the peak shape and performed poorly during the falling edge smoothing process. The distortion of signals is acceptable in neutron and gamma-ray discrimination applications if the pulse shape difference between the neutrons and gamma rays is successfully preserved or amplified after the filtering process.

The objective evaluation results for the three best filters of the PCNN and LG are presented in Tables 2 and 3, respectively. The detailed experimental results for all filters coupled with the PCNN and LG are presented in Sect. S3 of Supplemental Information.

Pertaining to the PCNN, the experimental results showed that the LMS and Wiener filters performed poorly

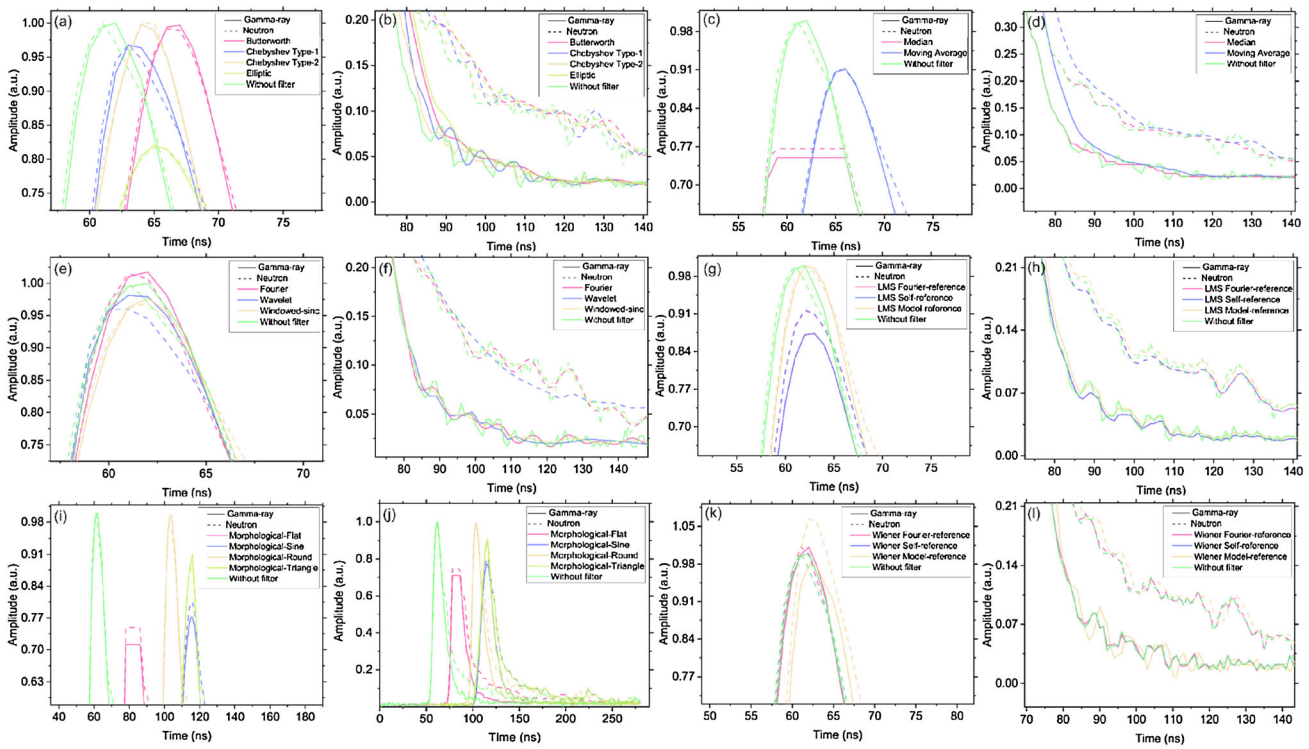

Fig. 4 (Color online) Peak and falling edge distortion. The solid line represents the gamma-ray pulse signals, and dotted line denotes the neutron pulse signals. Filters with fewer signal distortion are preferred under the same discrimination performance

Table 2 Filtering performance of the three best filters of PCNN

Filtering methods	Evaluation criteria					
Wavelet	FoM	MSE	PSNR	RMSE	DIV	ED
	2.5915	7.83×10^{-5}	41.4729	0.0086	0.0232	0.0233
	Distort	N-count	G-count	Error	Error ratio	Time (s)
	0.0187	2050	7364	13	0.0014	5.7782
Elliptic	FoM	MSE	PSNR	RMSE	DIV	ED
	2.1942	0.0053	22.7510	0.0728	0.1717	0.1567
	Distort	N-count	G-count	Error	Error ratio	Time (s)
	0.1848	2065	7349	28	0.0030	1.2646
Median	FoM	MSE	PSNR	RMSE	DIV	ED
	2.1811	0.0007	31.7574	0.0264	0.1937	0.0624
	Distort	N-count	G-count	Error	Error ratio	Time (s)
	0.2231	2088	7326	51	0.0054	0.2351

regardless of the reference signal used. The time consumption of their model-reference conditions is inferior because it takes a considerable amount of time to fit 9414 pulse signals using the three-decay-exponential function. Although the filtered signals of these two filters are the most similar to the original signals, with the best denoised signal similarity measurements, they failed to preserve the difference between neutrons and gamma rays and hence showed an unsatisfactory discrimination effect. The moving average filter had the shortest discrimination time while presenting an acceptable discrimination performance. The Fourier filter is the most balanced filter, which showed good discrimination results and the best denoised signal similarity.

Furthermore, the three filters with the best discrimination performance, that are wavelet, elliptic, and median, are shown in Table 2. The wavelet filter presented the FoM, which significantly outperformed the other filters. It also has small signal distortion and a low discrimination error. The only drawback is that its time consumption is not the highest among all the filtering methods. The elliptic filter has the second-best discrimination performance, low

Table 3 Filtering performance of the three best filters of LG

Filtering methods	Evaluation criteria					
Elliptic	FoM	MSE	PSNR	RMSE	DIV	ED
	2.1956	0.0143	18.447	0.1196	0.1200	0.1400
	Distort	N-count	G-count	Error	Error ratio	Time (s)
	0.1201	1929	7485	126	0.0134	1.2646
Moving Average	FoM	MSE	PSNR	RMSE	DIV	ED
	1.6637	0.0063	22.0353	0.0791	0.0959	0.0759
	Distort	N-count	G-count	Error	Error ratio	Time (s)
	0.0926	1899	7515	150	0.0159	0.1897
Wavelet	FoM	MSE	PSNR	RMSE	DIV	ED
	1.6587	7.83×10^{-5}	41.4729	0.0086	0.0232	0.0233
	Distort	N-count	G-count	Error	Error ratio	Time (s)
	0.0187	2000	7414	107	0.0114	5.7782

discrimination error, and a short filtering time requirement. The main disadvantage of this filter is that its parameters need to be reset for different neutron sources or scintillators, which makes its application inconvenient. The median filter showed the third-best discrimination performance and the second-best filtering time. The major drawback of this filter is that signal distortion is relatively high.

LG cannot discriminate the n-γPSs when coupled with morphological filters, with low FoM, high error, and massive time consumption. The morphological filters completely changed the pulse shape's characteristics to which LG was sensitive. Without the integration process, the LG cannot manage heavily distorted signals, unlike the PCNN. The same signal distortion problem leads to poor performance of the median filter. Furthermore, LG exhibits poor performance when coupled with Wiener, LMS, Fourier, Butterworth, and Chebyshev Type-2 filters. This is because the LG method has an intrinsic anti-noise ability, which is attributed to the noise-processing ability of the QC-SCM. This good anti-noise ability makes it unable to benefit significantly from the noise reduction effect of these filters while suffering from the negative influence caused by information loss during the filtering process.

Table 3 lists the filters with the best discrimination performance (elliptic, moving average, and wavelet). The elliptic filter exhibited the best discrimination performance, with the highest FoM, minimal signal distortion, and fast discrimination time. The primary disadvantage is the manual parameters. The moving average filter achieved the lowest time consumption and the second-best FoM. Finally, the wavelet filter presented the best discrimination performance and denoised signal similarity. The primary drawback of this method is its high computational complexity.

6 Conclusion

This study proposes an LG method for neutron and gamma-ray pulse-shape discrimination. This method uses a computationally convenient process, that is, the ladder gradient calculation process, to obtain the discrimination factor. Furthermore, QC-SCM was proposed to generate the ignition maps required by the ladder gradient calculation. Experiments were conducted to compare the proposed method with five other discrimination methods: falling edge percentage slope, zero crossing, charge comparison, frequency gradient analysis, and pulse-coupled neural network. The experimental results demonstrate the robustness and efficacy of the LG method, with the second-best FoM and low computational complexity.

Moreover, the filter adaptability of the PCNN and LG methods was investigated. Their performance was evaluated using both subjective figures and objective evaluation criteria. The evaluation criteria had the following four aspects:

- discrimination performance (FoM)
- denoised signal similarity (signal-to-noise ratio, mean square error, root mean square error, DIV, and entropy difference)
- time (total time consumption for each filter to process all 9414 signals)
- discrimination accuracy (neutron pulse signal count, gamma-ray pulse signal count, error, and error ratio)

The advantages and disadvantages of various filters and the possible reasons for their adaptability were analyzed. The experimental results revealed that the wavelet, elliptic, and median filters were the most adaptive of the PCNN; and the elliptic, moving average, and wavelet filters were the most suitable for the LG. In future research, the LG method will be further optimized and implemented on integrated radiation detection systems, and the LG

parameters will be studied to provide an automatic parameter LG method.

Author contributions All authors contributed to the study conception and design. Material preparation, data collection and analysis were performed by Hao-Ran Liu, Ming-Zhe Liu and Yu-Long Xiao. The first draft of the manuscript was written by Hao-Ran Liu, and all authors commented on previous versions of the manuscript. All authors read and approved the final manuscript.

References

1. T. Bily, L. Keltnerova, Non-linearity assessment of neutron detection systems using zero-power reactor transients. Appl. Radiat. Isotopes **157**, 109016 (2020). https://doi.org/10.1016/j.apradiso.2019.109016
2. E. Rohée, R. Coulon, C. Jammes et al., Delayed Neutron detection with graphite moderator for clad failure detection in sodium-cooled fast reactors. Ann. Nucl. Energy **92**, 440–446 (2016). https://doi.org/10.1016/j.anucene.2016.02.003
3. V. Yanchukovsky, V. Kuz'menko, Method of automatic correction of neutron monitor data for precipitation in the form of snow in real time. Solar-Terr. Phys. **7**, 114–120 (2021). https://doi.org/10.12737/stp-73202108
4. R.T. Kouzes, J.H. Ely, L.E. Erikson et al., Neutron detection alternatives to 3He for national security applications. Nucl. Instrum. Methods Phys. Sect. A **623**, 1035–1045 (2010). https://doi.org/10.1016/j.nima.2010.08.021
5. D. VanDerwerken, M. Millett, T. Wilson et al., Meteorologically driven neutron background prediction for homeland security. IEEE Trans. Nucl. Sci. **65**, 1187–1195 (2018). https://doi.org/10.1109/TNS.2018.2821630
6. A. Soto, R.G. Fronk, K. Neal et al., A semiconductor-based neutron detection system for planetary exploration. Nucl. Instrum. Methods Phys. Sect. A **966**, 163852 (2020). https://doi.org/10.1016/j.nima.2020.163852
7. M. Haertlein, M. Moulin, J.M. Devos *et al.*,in *Methods in Enzymology* Vol. 566 (ed Zvi Kelman) 113–157, Academic Press, 2016
8. Y. Kavun, T. Eyyup, M. Şahan et al., Calculation of production reaction cross section of some radiopharmaceuticals used in nuclear medicine by new density dependent parameters. Süleyman Demirel Üniversitesi Fen Edebiyat Fakültesi Fen Dergisi **14**, 57–61 (2019). https://doi.org/10.29233/sdufeffd.477539
9. F.D. Brooks, Development of organic scintillators. Nucl. Instrum. Methods **162**, 477–505 (1979). https://doi.org/10.1016/0029-554X(79)90729-8
10. D. Cester, M. Lunardon, G. Nebbia et al., Pulse shape discrimination with fast digitizers. Nucl. Instrum. Methods Phys. Sect. A **748**, 33–38 (2014). https://doi.org/10.1016/j.nima.2014.02.032
11. M.L. Roush, M.A. Wilson, W.F. Hornyak, Pulse shape discrimination. Nucl. Instrum. Methods **31**, 112–124 (1964). https://doi.org/10.1016/0029-554X(64)90333-7
12. B. Liu, M. Liu, M. He et al., Model-based pileup events correction via kalman-filter tunnels. IEEE Trans. Nucl. Sci. **66**, 528–535 (2019). https://doi.org/10.1109/TNS.2018.2885074
13. Y. Huang, M. Liu, R. Luo et al., Neutron–gamma pulse pileup correction based on mathematical morphology and optimized grey model. Nucl. Instrum. Methods Phys. Sect. A **1014**, 165739 (2021). https://doi.org/10.1016/j.nima.2021.165739
14. D. Wolski, M. Moszyński, T. Ludziejewski et al., Comparison of n-γ discrimination by zero-crossing and digital charge comparison methods. Nucl. Instrum. Methods Phys. Sect. A **360**, 584–592 (1995). https://doi.org/10.1016/0168-9002(95)00037-2
15. P. Sperr, H. Spieler, M.R. Maier et al., A simple pulse-shape discrimination circuit. Nucl. Instrum. Methods **116**(55–59), 1974 (1974). https://doi.org/10.1016/0029-554X(74)90578-3
16. S. Pai, W.F. Piel, D.B. Fossan et al., A versatile electronic pulse-shape discriminator. Nucl. Instrum. Methods Phys. Sect. A **278**, 749–754 (1989). https://doi.org/10.1016/0168-9002(89)91199-6
17. G. Liu, M.J. Joyce, X. Ma et al., A digital method for the discrimination of neutrons and γ rays with organic scintillation detectors using frequency gradient analysis. IEEE Trans. Nucl. Sci. **57**(1682–1691), 2010 (2010). https://doi.org/10.1109/TNS.2010.2044246
18. M. Liu, B. Liu, Z. Zuo et al., Toward a fractal spectrum approach for neutron and gamma pulse shape discrimination. Chin. Phys. C **40**, 066201 (2016). https://doi.org/10.1088/1674-1137/40/6/066201
19. H. Liu, Y. Cheng, Z. Zuo et al., Discrimination of neutrons and gamma rays in plastic scintillator based on pulse-coupled neural network. Nucl. Sci. Tech. **32**, 82 (2021). https://doi.org/10.1007/s41365-021-00915-w
20. R. Eckhorn, H.J. Reitboeck, M. Arndt et al., Feature linking via synchronization among distributed assemblies: simulations of results from cat visual cortex. Neural Comput. **2**, 293–307 (1990). https://doi.org/10.1162/neco.1990.2.3.293
21. W.J. Freeman, B.W. van Dijk, Spatial patterns of visual cortical fast EEG during conditioned reflex in a rhesus monkey. Brain Res. **422**, 267–276 (1987). https://doi.org/10.1016/0006-8993(87)90933-4
22. R. Eckhorn, R. Bauer, W. Jordan et al., Coherent oscillations: A mechanism of feature linking in the visual cortex? Biol. Cybern. **60**, 121–130 (1988). https://doi.org/10.1007/BF00202899
23. A.L. Hodgkin, A.F. Huxley, A quantitative description of membrane current and its application to conduction and excitation in nerve. J. Physiol. **117**, 500–544 (1952). https://doi.org/10.1113/jphysiol.1952.sp004764
24. H. Liu, M. Liu, D. Li et al., Recent advances in pulse-coupled neural networks with applications in image processing. Electronics **11**(20), 3264 (2022). https://doi.org/10.3390/electronics11203264
25. H.S. Ranganath, G. Kuntimad, Object detection using pulse coupled neural networks. IEEE Trans. Neural Netw. **10**, 615–620 (1999). https://doi.org/10.1109/72.761720
26. B. Yu, L. Zhang, Pulse-coupled neural networks for contour and motion matchings. IEEE Trans. Neural Netw. **15**, 1186–1201 (2004). https://doi.org/10.1109/TNN.2004.832830
27. X. Gu, D. Yu, L. Zhang, Image shadow removal using pulse coupled neural network. IEEE Trans. Neural Networks **16**, 692–698 (2005). https://doi.org/10.1109/TNN.2005.844902
28. J.L. Johnson, Pulse-coupled neural nets: translation, rotation, scale, distortion, and intensity signal invariance for images. Appl. Opt. **33**, 6239–6253 (1994). https://doi.org/10.1364/AO.33.006239
29. H. Liu, Z. Zuo, P. Li et al., Anti-noise performance of the pulse coupled neural network applied in discrimination of neutron and gamma-ray. Nucl. Sci. Tech. **33**, 75 (2022). https://doi.org/10.1007/s41365-022-01054-6
30. Z. Zuo, H. Liu, Y. Yan et al., Adaptability of n–γ discrimination and filtering methods based on plastic scintillation. Nucl. Sci. Tech. **32**, 28 (2021). https://doi.org/10.1007/s41365-021-00865-3
31. Z. Yang, M. Dong, Y. Guo et al., A new method of microcalcifications detection in digitized mammograms based on improved simplified PCNN. Neurocomputing **218**, 79–90 (2016). https://doi.org/10.1016/j.neucom.2016.08.068
32. D.A. Winter, H.G. Sidwall, D.A. Hobson, Measurement and reduction of noise in kinematics of locomotion. J. Biomech.

7(157–159), 1974 (1974). https://doi.org/10.1016/0021-9290(74)90056-6
33. K.S. Erer, Adaptive usage of the Butterworth digital filter. J. Biomech. **40**(2934–2943), 2007 (2007). https://doi.org/10.1016/j.jbiomech.2007.02.019
34. D.G.E. Robertson, J.J. Dowling, Design and responses of Butterworth and critically damped digital filters. J. Electromyogr. Kinesiol. **13**, 569–573 (2003). https://doi.org/10.1016/S1050-6411(03)00080-4
35. M.K. Anju, M. Katiyar, Design of butterworth and chebyshev1 lowpass filter for equalized group delay. *International J. Advanced Research in Computer Science and Software Engineering* **2**, 524–528 (2012)
36. W.M. Laghari, M.U. Baloch, M.A. Mengal et al., Performance analysis of analog butterworth low pass filter as compared to chebyshev type-I filter, chebyshev type-II filter and elliptical filter. Circuits Syst. **5**(9), 8 (2014). https://doi.org/10.4236/cs.2014.59023
37. G. Arce, M. McLoughlin, Theoretical analysis of the max/Median filter. IEEE Trans. Acoustics, Speech, and Signal Processing **35**, 60–69 (1987). https://doi.org/10.1109/TASSP.1987.1165036
38. J. Wang, J. Liang, F. Gao et al., A method to improve the dynamic performance of moving average filter-based PLL. IEEE Trans. Power Electron. **30**, 5978–5990 (2015). https://doi.org/10.1109/TPEL.2014.2381673
39. A. Loukas, A. Simonetto, G. Leus, Distributed autoregressive moving average graph filters. IEEE Signal Process. Lett. **22**, 1931–1935 (2015). https://doi.org/10.1109/LSP.2015.2448655
40. J. Allen, Short term spectral analysis, synthesis, and modification by discrete Fourier transform. IEEE Trans. Acoust. Speech Signal Proces. **25**, 235–238 (1977). https://doi.org/10.1109/TASSP.1977.1162950
41. T.T. Cai, On block thresholding in wavelet regression: Adaptivity, block size, and threshold level. Stat. Sin. 1241–1273 (2002)
42. D.L. Donoho, Progress in wavelet analysis and WVD: a ten minute tour. Prog. Wavelet Anal. Appl. 109–128 (1993)
43. D.L. Donoho, De-noising by soft-thresholding. IEEE Trans. Inf. Theory **41**, 613–627 (1995). https://doi.org/10.1109/18.382009
44. D.L. Donoho, I.M. Johnstone, G. Kerkyacharian et al., Wavelet shrinkage: Asymptopia? J. R. Stat. Soc. Ser. B (Methodol.) **57**, 301–337 (1995). https://doi.org/10.1111/j.2517-6161.1995.tb02032.x
45. K.M. Indrebo, R.J. Povinelli, M.T. Johnson, Minimum Mean-Squared Error Estimation of Mel-Frequency Cepstral Coefficients Using a Novel Distortion Model. IEEE T.rans Audio Speech Lang. Process. **16**, 1654–1661 (2008). https://doi.org/10.1109/TASL.2008.2002083 (2008)
46. E.A. Robinson, S. Treitel, Principles of digital wiener filtering*. Geophys. Prospect. **15**, 311–332 (1967). https://doi.org/10.1111/j.1365-2478.1967.tb01793.x
47. This is a book S. Haykin, B. Widrow, *Least-mean-square adaptive filters*. Vol. 31 John Wiley & Sons (2003)
48. P. Maragos, R. Schafer, Morphological filters–Part I: their set-theoretic analysis and relations to linear shift-invariant filters. IEEE Trans. Acoust. Speech Signal Process. **35**(1153–1169), 1987 (1987). https://doi.org/10.1109/TASSP.1987.1165259
49. P. Maragos, R. Schafer, Morphological filters—part II: their relations to median, order-statistic, and stack filters. IEEE Trans. Acoust. Speech Signal Process. **35**, 1170–1184 (1987). doi:https://doi.org/10.1109/TASSP.1987.1165254 (1987).
50. D. Zhang, T. Phung, J. Fletcher et al., Windowed-sinc band-pass filter based reference signal extraction for grid synchronization. Int. J. Electr. Energy **1**, 23–28 (2013). https://doi.org/10.12720/ijoee.1.1.23-28
51. D. Zhang, E. Ambikairajah, H. Niu, Application of windowed-sinc band-pass filter to accurate and fast calculation of impedance for digital distance relaying. Int. J. Signal Process. Syst. **1**(2), 250–255 (2013). https://doi.org/10.12720/ijsps.1.2.250-255
52. R.A. Winyard, J.E. Lutkin, G.W. McBeth, Pulse shape discrimination in inorganic and organic scintillators. I. Nucl. Instrum. Methods **95**(141–153), 1971 (1971). https://doi.org/10.1016/0029-554X(71)90054-1
53. M. Diwakar, M. Kumar, A review on CT image noise and its denoising. Biomed. Signal Process. Control **42**, 73–88 (2018). https://doi.org/10.1016/j.bspc.2018.01.010
54. J. Lin, Divergence measures based on the Shannon entropy. IEEE T. Inf. Theory **37**(145–151), 1991 (1991). https://doi.org/10.1109/18.61115
55. P. Bromiley, N. Thacker, E. Bouhova-Thacker, Shannon entropy, renyi entropy, and information. Stat. Inf. Series (2004–004) **9** (2004)
56. J. Iwanowska-Hanke, M. Moszynski, L. Swiderski et al., Comparative study of large samples (2“ × 2”) plastic scintillators and EJ309 liquid with pulse shape discrimination (PSD) capabilities. J. Instrum. **9**, P06014 (2014). https://doi.org/10.1088/1748-0221/9/06/p06014
57. Z. Zuo, Y. Xiao, Z. Liu et al., Discrimination of neutrons and gamma-rays in plastic scintillator based on falling-edge percentage slope method. Nucl. Instrum. Methods Phys. Sect. A **1010**, 165483 (2021). https://doi.org/10.1016/j.nima.2021.165483
58. Y. Lotfi, S.A. Moussavi-Zarandi, N. Ghal-Eh et al., Optimization of pulse processing parameters for digital neutron-gamma discrimination. Radiat. Phys. Chem. **164**, 108346 (2019). https://doi.org/10.1016/j.radphyschem.2019.108346
59. N.P. Hawkes, K.A.A. Gamage, G.C. Taylor, Digital approaches to field neutron spectrometry. Radiat. Meas. **45**, 1305–1308 (2010). https://doi.org/10.1016/j.radmeas.2010.06.043